

Optimize the corrosion behavior of AISI 204Cu stainless steel in different environments under previous cold working and welding

Haider Mahdi Lieth, Murtadha Abbas Jabbar, Raad Jamal Jassim, and Raheem Al-Sabur* 

Department of Mechanical Engineering, College of Engineering, University of Basrah, Basrah, Iraq

Received: 3 February 2023 / Accepted: 4 July 2023

Abstract. Enhancing corrosion resistance in stainless-steel alloys is a paramount objective in the petroleum industry. This study investigated the effects of the previous cold working and welding processes on the mechanical properties and corrosion rates of 204 Cu stainless steel in different aggressive environments (crude oil, freshwater, and seawater). The experimental sets were supported by microstructure analysis. The mean weight loss method was employed to determine the corrosion rates, which were optimized using the Taguchi method. The ferrite and austenite phase bands, as well as the deformed portions of austenite, are pushed to flatten out during cold working, which increases the material's hardness. Cold-worked steels were welded, creating an annealed area around the HAZ in addition to the usual weld zones, which demonstrated partial microstructure recovery and hardness reduction. HAZ showed signs of iron overload and chromium nitride precipitation. Cold-worked specimens only showed reduced corrosion resistance to 30% of the initial rate and reduced thickness. Moreover, the Taguchi optimization technique indicated that the corrosion environment has the most effect on the corrosion rate compared to the cold work ratio for welded and non-welded stainless-steel specimens.

Keywords: cold working / AISI 204Cu stainless steel / corrosion behavior / Taguchi methods

1 Introduction

The recent technological developments in rolling and smelting increased the reinforcements of high-strength stainless steel [1]. The highly competitive cost and steady increase in low nickel-inforced stainless steel strongly support reinforcement techniques [2]. AISI 204Cu is a low-nickel austenite stainless steel where Mn and N elements replace a portion of the Ni component. Compared to AISI 204Cu and AISI 304, both alloys have the same corrosion resistance, but the formability is better in AISI 204Cu, and its cost is highly competitive [3]. AISI 204Cu is widely utilized in anticorrosion products such as kitchen utensils, electrical components, automotive parts, and construction materials [4,5]. As a high-corrosion-resistant material, AISI 204Cu was introduced in 2001 to replace AISI 304 stainless steel [6]. Due to the alloy's presence of copper (2.72%), the austenitic crystal structure is permanent in AISI 204Cu stainless steel. Because of the high copper content in AISI 204Cu stainless steel, the nickel content can be kept low at an estimated 1.97% [7], which lowers manufacturing costs. Copper enhances the overall resistance of corrosion in

acidic environments and pitting corrosion resistance in environments containing chloride [8,9]. Austenitic stainless steel's yield point can be extremely improved by cold deformation, that is, plastic deformation at ambient temperature [10]. The austenitic 204Cu cold-worked stainless steel is characterized by the martensitic transformation that results from cold-working, where the austenite in this steel is stable at ambient temperature [11,12]. Additionally, the presence of spherical copper particles in the microstructure of austenite, which gives it a stronger hardness, explains the stability of austenite in stainless steel AISI 304 [13].

The austenitic stainless steel welding process has special requirements compared to ordinary steel alloys [14]. It has a thermal expansion of 50% more than normal steel [15] and low thermal and electrical conductivity [16]. Moreover, in austenitic stainless-steel welding, the heat is not going away very quickly, so a little heat is needed to perform the welding [17]. Failure to adopt some welding requirements leads to several problems that affect the quality and performance of the weld joint. Intergranular corrosion results from sensitization of the weld's heat-affected zone (HAZ), which in turn causes, when heated between 427 and 871 °C, chromium carbide to form and precipitate at grain boundaries in the HAZ, which results in

* e-mail: raheem.musawel@uobasrah.edu.iq

Table 1. Chemical composition of AISI 204Cu stainless steel (wt.%).

Fe	C	Si	Mn	Cr	Ni	Cu	P	S	Co
Bal.	0.087	0.31	8.82	14.9	1.03	1.75	0.048	0.034	0.049

sensitization [17]. In contrast, hot cracking occurs due to the penetration of phosphorous and sulfur in the grain boundaries due to the low melting temperature [16].

Using plastic deformation to strengthen the materials is known as cold working [18,19]. It occurs due to decreasing dislocation mobility during the materials' plastic deformation, and it is an important method for increasing the strength of steel [20]. It can be done as a percentage such as 10%, 20%...etc., where it was discovered that increasing the cold-working level for austenitic stainless steels led to improvements in both tensile and yield strength [21].

Despite several studies on the corrosion rates of 204Cu austenitic stainless steel, research on the effects of pre-cold working and pre-welding on 204Cu corrosion rates are rare. The current study clarifies these effects at various levels in different corrosive environments. Furthermore, mechanical characteristics and microstructure were investigated in each environment, and the optimum process parameters were studied.

2 Experimental work

2.1 Raw materials and cold workings

Two AISI 204Cu stainless steel rods, each measuring 12 mm in diameter and 3.6 m in length, were selected. The chemical composition was measured using a PECTROT-EST TXC25 spectrometer, as shown in Table 1.

The specimens were divided into three groups and exposed to cold working percentages of 10%, 20%, and 30%, respectively, using a universal tensile machine according to ASTM E8M [22]. On the other hand, a certified welder cut several specimens and rejoined them using the welding process. Then the welded samples were divided into three groups and exposed to cold working, similar to the previous case. The hardness test they were made following ASTM E384 [23]. The 63 tensile test specimens were divided into seven cases according to cold working levels (the first case as received, the next three cases without welding, and the rest three cases with welding); each division contains nine specimens, three for each corrosive environment (crude oil, freshwater, and seawater). In the first case, the specimens were kept without any processing, while the others were exposed to the cold working of 10%, 20%, and 30%, respectively, as shown in Figures 1 and 2. After machining the metal, it was annealed to relieve the cold-working and machining stresses. The annealing procedure was used to produce 204Cu stainless steel. Type 204 is immersed at 1038–1121 °C and quenched in water or air [24].

2.2 Aggressive environments

Three corrosive media were used to determine the effect of pre-cold and welding on the corrosion resistance of the AISI 204Cu stainless steel. The corrosive environment is crude oil, freshwater, and seawater. Table 2 shows the properties of the crude oil used in the experiment, while the properties of fresh water and seawater are listed in Table 3. It should be noted here that the Arabian Gulf region has been adopted for the properties of seawater, including the pH, as the Iraqi ports are linked to this sea outlet only.

2.3 Welding and corrosion test

Double-V joint configuration welding specimens were prepared using a lathe machine, and a heating apparatus was utilized to eliminate the specimens' moisture. In addition, many welding requirements have been considered, such as eliminating organic impurities, greases, cutting agents, and pencil marks [17]. In the welding process, an electrode of 316L stainless steel was used. According to the standard ASTM G31 [25], the loss-weight method was used to investigate the corrosion of the specimens. The specimens were properly cleaned, where the impurities and the oxidization layer (if it exists) were removed using chemical and mechanical cleaners. A special container was used for the corrosion test, and a suitable test period was selected to overcome the inaccuracy and misleading results of short-period tests. The tests were prepared as seven cases immersed in different crude oil, freshwater, and seawater environments. The container was firmly closed and stored for seven days. The specimens were extracted weekly and cleaned to calculate the lost weight. The equation below was used to calculate the corrosion rate (CR):

$$CR = \frac{\Delta m \times 24 \times 365 \times 10}{\rho \times A \times st}, \quad (1)$$

where CR is the corrosion rate in mils per year (MPY), Δm is weight loss in milligrams, ρ is metal density in g/cm^3 , A is the area of the specimen in cm^2 , and t is the time of exposure in hours.

2.4 Experimental design

The Taguchi method is considered one of the best methods used during the last six decades for improving the quality of outputs by using the least possible number of experiments [26,27]. The Taguchi as a systematic process optimization approach involves several steps: problem definition, design

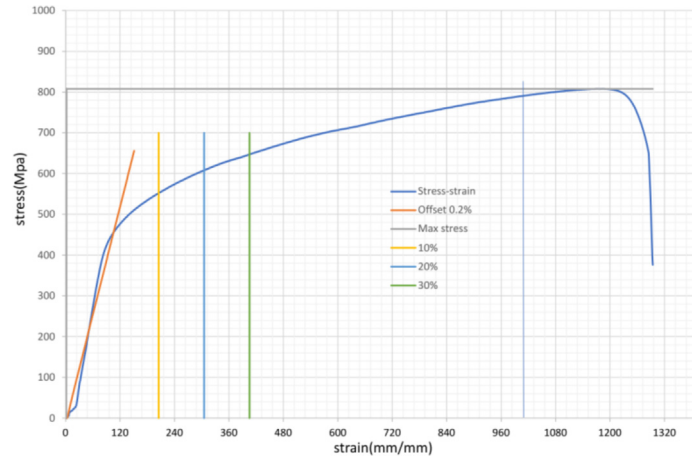


Fig. 1. Stress strain curve of 204Cu stainless steel with the cold working.

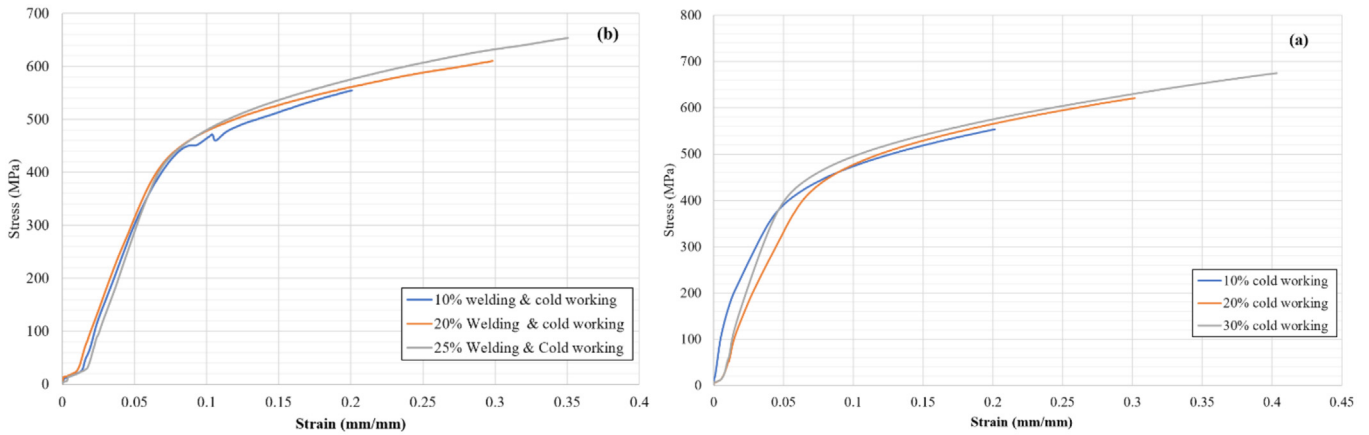


Fig. 2. Stress strain curves of 204Cu stainless steel (a) cold working without welding, (b) cold working with welding.

Table 2. Properties of crude oil.

Test	Results	Method
Density at 15 °C (g/cm ³)	0.97	ASTM D-1298
Flash point °C	138.00	ASTM D-93
Kinematic viscosity (m ² /s)	370.70	ASTM D-445
Pour point (°C)	-3.00	ASTM D-97
Sulphur content (wt%)	4.63	ASTM D-4294
Carbon residue (RAMS) (wt%)	9.52	ASTM D-524
Water & sediment (vol%)	0.10	ASTM D-1796

Table 3. Properties of fresh water and sea water.

Test	Freshwater	Seawater
Temperature (°C)	18.00	16.00
Mass density (kg/m ³)	998.72	1027.03
Kinematic viscosity (m ² /s)	1.0435E-06	1.1978E-06
pH	9.5	8.12
Dynamic viscosity (Pa.s)	0.001075	0.001234

of experiments (DOE), parameter selection, conducting experiments, analysis, optimization, and verification. With several experiments, the DOE effectively explores the parameter space using orthogonal arrays. This technique often focuses on the orthogonal array (OA) for variance reduction and the signal-to-noise ratio (S/N) to estimate the deviations of the values [28]. The (S/N) concept assesses the acquired data, evaluates variation, and determines the ideal factor levels. The technique lowers

noise sensitivity, ensures resilience, and raises quality. The Taguchi method makes it possible to efficiently explore, optimize, and enhance the performance of products or processes.

In Taguchi's method, three types of S/N ratios can be used depending on the nature of the required optimized parameter, such as:

For Smaller-the-Better S/N ratio:

$$S/N = -10 \log \left(\frac{1}{n} \sum_i^n y^2 \right). \quad (2)$$

Table 4. Parameters and their levels in the experimental design.

Exp. no	Corrosive medium	Cold working (%)
1	Freshwater	10%
2	Freshwater	20%
3	Freshwater	30%
4	Sea water	10%
5	Sea water	20%
6	Sea water	30%
7	Crude oil	10%
8	Crude oil	20%
9	Crude oil	30%

For Larger-the-Better

$$S/N = -10 \log \left(\frac{1}{n} \sum_i^n \frac{1}{y_i} \right). \quad (3)$$

For Nominal-the-Best S/N ratio:

$$S/N = -10 \log \left(\frac{\bar{y}^2}{s^2} \right), \quad (4)$$

where n represents the experimental sets, and y_i represents each run's observed response values. This study utilized the S/N ratio "smaller-the-better" to determine the optimal parameters of interest. The S/N ratio was calculated using Minitab 19.

Taguchi's design optimized the process parameters for a minimum 204Cu stainless steel bars corrosion rate. Three levels were used for two parameters. In studies on corrosion rate, the results are often discussed in three different environments: crude oil, freshwater, and seawater [29], and this matter was also adopted in this study as the first parameter. The second parameter is the cold working percentage ratio of 10%, 20%, and 30%, as shown in Table 4. This study's lower value is best relied on for the S/N ratio, and the results were analyzed using Minitab 19 software.

3 Results and discussion

3.1 Microhardness

Figure 3 shows the microhardness results of the cold-working 204Cu austenitic stainless steels. The microhardness values were measured at room temperature following the cold-working and welding. Therefore, all of the changes in microhardness were due to cold working.

For both specimens that are strengthened by cold working only and those in which welding was added, the achieved hardness values are higher than the average hardness area of 204Cu, which is 300–350 HV, and also higher than the average hardness area of ordinary stainless steel, which is 200–250 HV [30]. This study examined three

samples for each set of experiments to get the mean values according to the standard deviation (STD). STD = 1 was used to find the "error bars", as indicated in Figure 3. By using three samples for each set of experiments, the analysis aimed to account for the repeatability of the outcomes. Estimating the mean values and STD qualified for analyzing the data dispersion and central tendency and dispersion. Using STD = 1 as the basis for the error bars in Figure 3 shows the importance of the associated measurement uncertainty. During the various cold working stages, a relative deformation occurs in the specimens, and the possibility of a phase transformation to martensite from austenite increases, which explains the hardness values [21]. In the case of welded and cold-worked specimens, they achieved higher hardness than the corresponding specimens without welding. Using a 316L stainless steel welding electrode in the specimens' welding process increased the hardness values in the welding area.

3.2 Microstructure

The microstructure of a specimen can have an extremely large impact on its chemical, physical, and mechanical properties. Figure 4a depicts the 204Cu stainless steel base metal microstructure; an austenite, ferrite matrix, and tiny twin-grain makeup are included. When the cold working was applied to the specimens, the austenite and ferrite phase bands flattened, and the austenite deformed, as shown in Figures 4a and 4d which led to improved hardness. Figures 4c and e indicated that the microstructures comprised primary ferrite (dark phase) dendrites with austenite (light phase) inner dendrites. It may result from the low carbon content of the welding filler material, which aligns with carbon operations to stabilize the austenite phase in welded metal [31].

The delta ferrite phase contained more chromium than the austenite phase in the sample, which was caused by the iron phase's stability. However, the amount of Ni and Mn in the sample was higher in the austenite phase than in the delta ferrite phase, which can be attributed to the austenitic phase's stability [31,32].

Even though the current study does not directly address the brittle-to-ductile fracture transition in the welding zone, the formation of delta structures in this region can potentially affect the resulting material fracture. The main functions of the transition from brittle to ductile fracture behavior are grain boundaries, phase distributions, and microstructural features. Therefore, it is reasonable to assume that the weld zone may display a change in fracture behavior from brittle to ductile due to the microstructural modifications brought on by cold working and welding, such as the creation of delta structures.

3.3 Surfaces analysis

The surface analysis and polishing objective was to examine the surface morphology of the 204Cu stainless steel samples and comprehend the impact of cold working and welding on the surface features. By investigating the

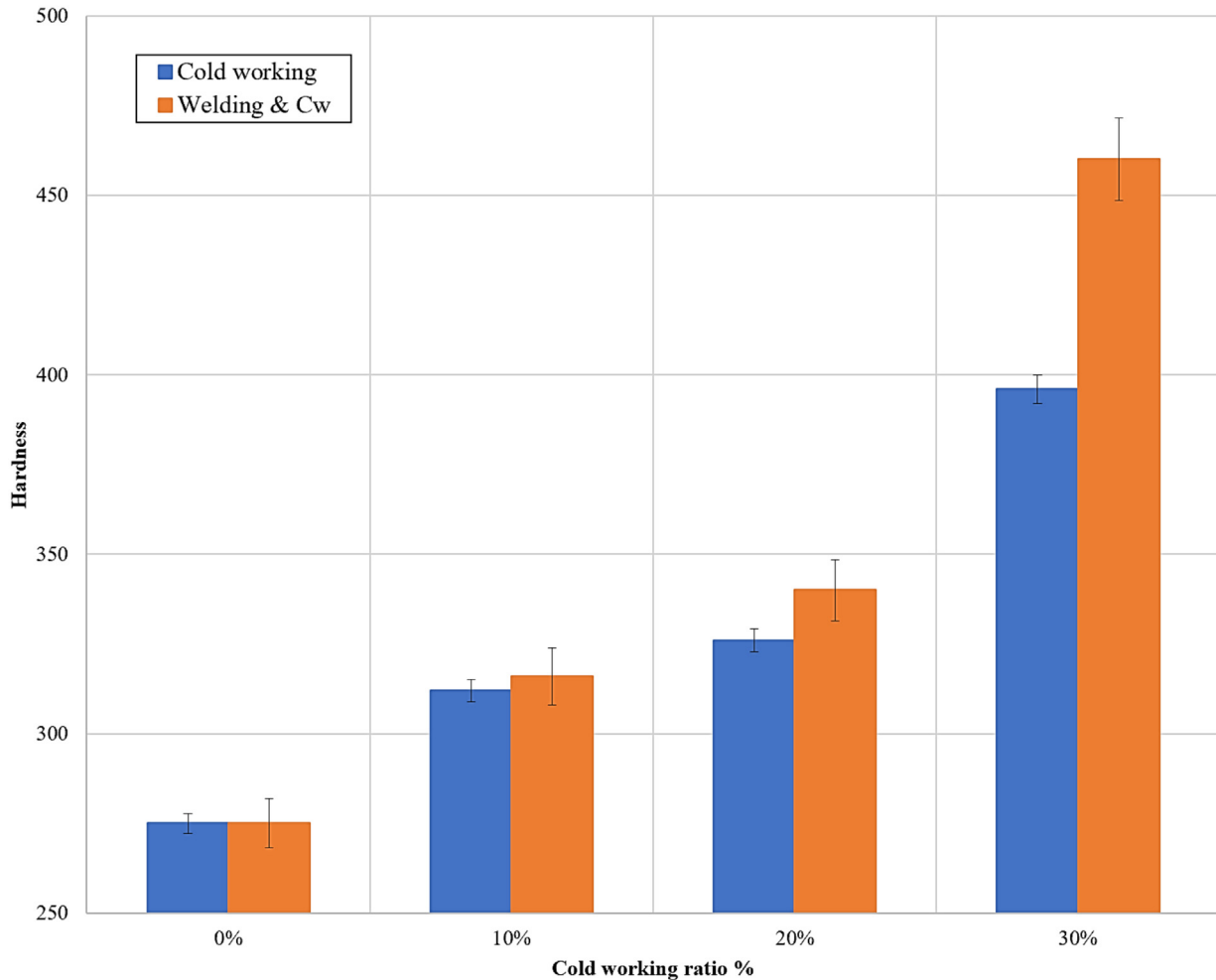


Fig. 3. Mean microhardness of 204Cu stainless steel with cold working ratio with and without welding (error bars = 1 standard deviation).

deviations in polished surface morphology, the differences caused by different cold working percentages and the further effect of welding on the material's surface structure can be assessed. These surface analyses discern the metal deformation degree due to cold working and welding, which can control the steel's mechanical properties and anticorrosion power.

High imaging resolution NanoSEM 450 scanning electron microscope (SEM) was used to investigate the surface morphology of the 204Cu stainless steel specimens. Figure 5 shows the variations in polished surface morphology for steel that has undergone 10%, 20%, and 20% cold working in addition to welding, respectively. The impact of cold working with varying proportions on the interior structure and the welding procedure appears obvious when examining the micro scanner images. The degree of deformation in the metal increases with the rate at which it is cold-worked, altering its mechanical properties, particularly its anti-corrosion capability. Welding has a greater impact on the metal's internal structure, which is reflected in the metal's corrosion resistance.

3.4 Corrosion rates

The mass difference from hostile environments is described earlier on the sample surfaces. The change in mass is a function of time for all specimens undergoing corrosion testing. Weight loss calculations provide a precise indication of corrosion rates. The weights before and after exposure to the corrosive medium were calculated using Equation 1.

Figures 6a and b explains the lost weight and corrosion rate in the seawater, where it was easily noticed that the highest weight loss was located in the received sample.

Regarding the corrosion rates, the highest sample was achieved at 30% cold working, while the as-received specimen achieved the least values. Moreover, the other specimens fluctuated depending on the immersion period.

When the specimens were immersed in the crude for four weeks, the overall corrosion rates were proportional to the increased cold-working ratios for the samples exposed to cold-working conditions, as shown in Table 5. Regarding the specimens that were welded and strengthened by cold

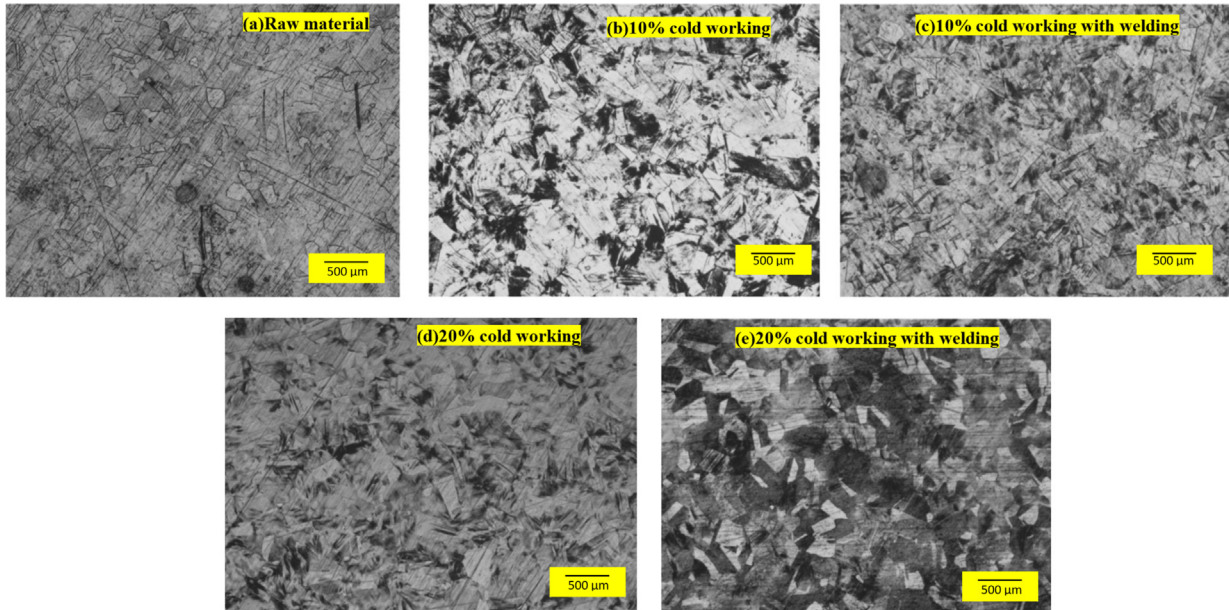


Fig. 4. Microstructure examination of 204Cu stainless steel (a) as-received steel; (b) 10% cold working; (c) 10% cold working with welding; (d) 20% cold working; and (e) 20% cold working with welding.

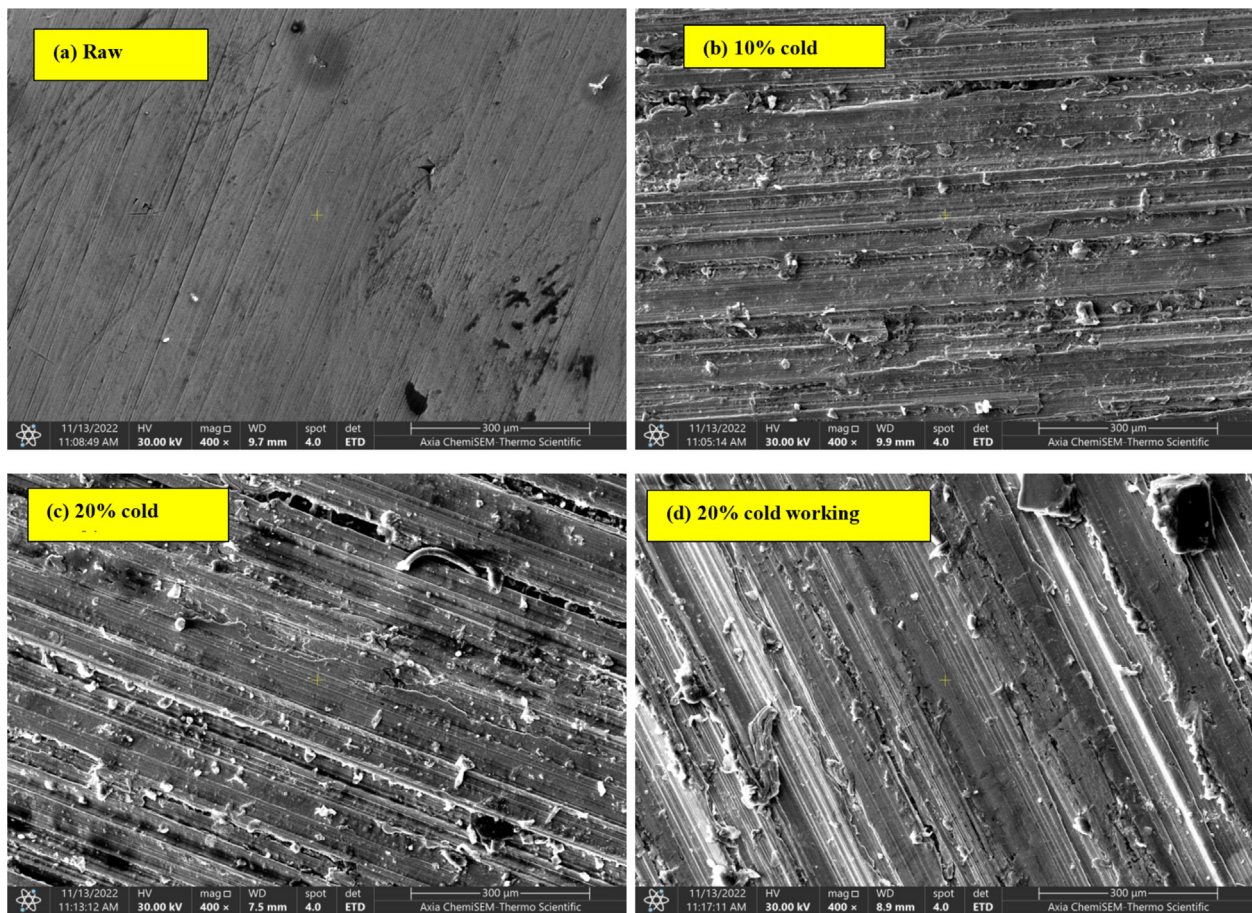


Fig. 5. SEM images for AISI 204Cu stainless steel: (a) as received steel; (b) 10% cold work; (c) 20% cold work with welding; (d) 30% cold work and welding.

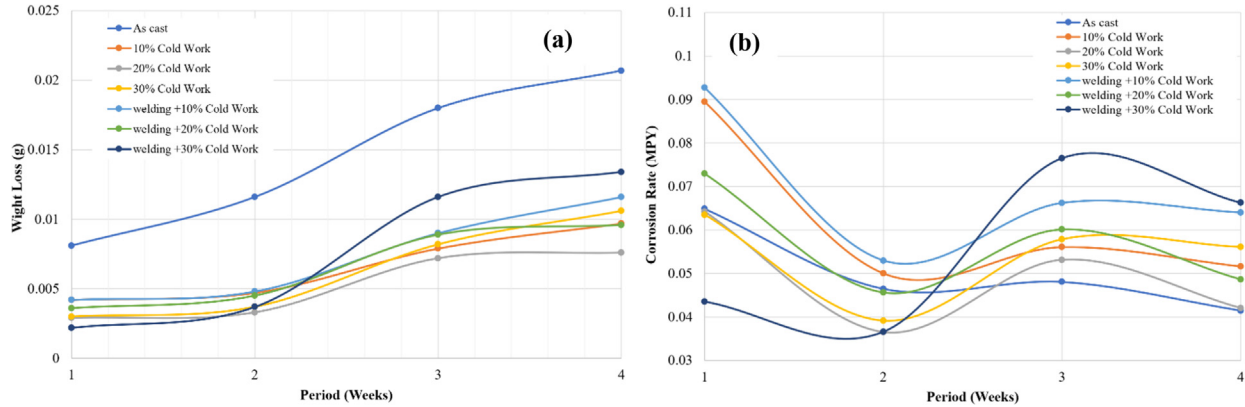


Fig. 6. Behavior of specimens in the seawater: (a) loss weight, (b) corrosion rate.

Table 5. Wight losses and corrosion rates in crude oil medium.

Specimens	Wight losses (g)				Corrosion rate (mm/year)
	1st week	2nd week	3rd week	4th week	
As cast	0.0033	0.0035	0.0169	0.0175	0.031486
10% Cold work	0.0043	0.0044	0.0118	0.0223	0.040481
20% Cold work	0.0019	0.002	0.0098	0.0111	0.029960
30% Cold Work	0.0016	0.0024	0.0082	0.0504	0.018406
Welding + 10% cold work	0.0018	0.0062	0.0067	0.0204	0.090306
Welding + 20% cold work	0.0008	0.004	0.0047	0.0188	0.088420
Welding + 30% cold work	0.0007	0.0034	0.0039	0.0092	0.046595

Table 6. Taguchi L9 orthogonal array for 204Cu stainless steel rod.

#	Corrosion Medium	Cold work %	Corrosion rate (mm/y)	S/N ratio
1	Fresh water	10	0.05034564	25.96
2	Fresh water	20	0.03765431	28.483
3	Fresh water	30	0.05176873	25.718
4	Sea water	10	0.061818325	24.177
5	Sea water	20	0.048986743	26.198
6	Sea water	30	0.054179653	25.323
7	Crude oil	10	0.029059979	30.734
8	Crude oil	20	0.024134118	32.347
9	Crude oil	30	0.052151476	25.654

work, the overall behavior for corrosion rates is not different from the previous samples; the only change that occurred was that the values of corrosion rates were higher than the corresponding non-welded specimens. The reason was that the welding process led to more deformations, defects, and distortions, which are considered sources of corrosion.

3.5 Taguchi results

3.5.1 Cold working strengthening

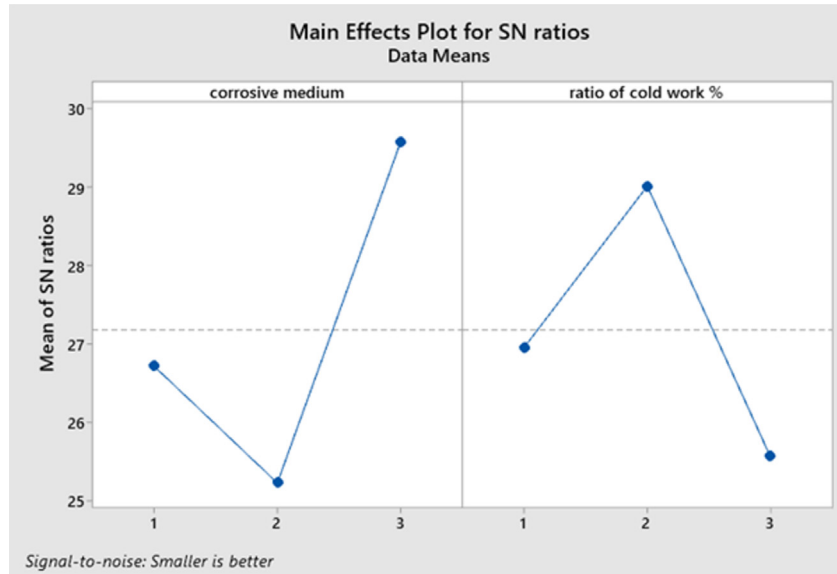
The Taguchi L9 orthogonal array experimental design was employed to identify the optimal conditions and to

evaluate the factor having the maximum significant effect on the corrosion rate of the 204Cu stainless steel rod by using MINITAB-19. The process parameters for the orthogonal array are described in Table 6.

ANOVA analysis was used to analyze the effect of each parameter on the resulting corrosion rates. As shown in Table 7 of the ANOVA analysis, the corrosion environment has the greatest significance because it has the highest F-value (4.46). Furthermore, the optimum predicted corrosion rates were achieved at crude oil for the specimens, which were 20% strengthened using a multi-response S/N ratio, as indicated in Figure 7.

Table 7. ANOVA analysis of 204Cu Stainless Steel Rod for cold working specimens.

Source	DF	Seq SS	Adj SS	Adj MS	<i>F</i>	<i>P</i>
corrosive medium	2	29.26	29.26	14.632	4.46	0.096
Cold work %	2	18.01	18.01	9.006	2.74	0.178
Residual error	4	13.13	13.13	3.282		
Total	8	60.41				

**Fig. 7.** Principal effects of S/N on 204Cu stainless steel corrosion rate.**Table 8.** ANOVA analysis of 204Cu stainless steel for welding and cold working specimens.

Source	DF	Seq SS	Adj SS	Adj MS	<i>F</i>	<i>P</i>
Corrosive medium	2	0.000541	0.000541	0.00027	17.87	0.01
Cold work %	2	0.000388	0.000388	0.000194	12.83	0.018
Residual error	4	0.000061	0.000061	0.000015		
Total	8	0.00099				

3.5.2 Welding and cold working strengthening

The specimens strengthened by welding and cold working do not have clear differences from the cold working. The optimum conditions were achieved at a 30% cold-working ratio and a crude oil environment. According to the ANOVA analysis of the corrosion rate, the corrosion environment has the greatest significance because it has the highest *F*-value (17.87) compared to the cold-working of corrosion, as shown in [Table 8](#).

Conclusions

In this study, AISI 204Cu stainless steel was strengthened using two ways. In the first case, the specimens were exposed to several cold working stages using the tensile

machine, and then the specimens were immersed in three different environments. The specimens were cut and then welded in the second case by arc welding. Later, these specimens were exposed to the same conditions as the first case. The important results are listed below.

- Cold working led to stress-induced twinning and deformation of the austenite phase, resulting in rapid grain splitting and a ribbon-type microstructure composed of austenite and ferrite grains. A well understanding of the microstructural modifications by cold working supports this observation, validating the findings.
- Using the Taguchi optimization approach, the crude oil environment gave the optimum process conditions for corrosion rate in stainless steel rods in both cases. The specimens that were 20% strengthened had the optimum

corrosion rate that was only cold worked before strengthening. In comparison, the specimens that were 30% strengthened gave the optimum corrosion rate when pre-welded and cold-worked before strengthening.

- As cold working is intensified, the hardness values rise correspondingly. The specimens undergo relative deformation during the various cold working steps, which raises the likelihood that austenite could phase change into martensite, which explains the hardness results. The effect of the welding process on the hardness values can also be seen since an increase in hardness values was evident due to the microstructure changes that occurred during the welding process.
- Corning environments are the most influential process parameters in determining corrosion rate. Following the major influence of aggressive media on corrosion behavior, this result is based on the observed variances in corrosion rates across various settings.

Acknowledgement. The authors would like to express their appreciation and sincere gratitude to the mechanical engineering and materials engineering departments in the College of Engineering at the University of Basrah.

References

1. Y. Yang, H. Qian, Y. Su, Effect of Mn addition on deformation behaviour of 23% Cr low nickel duplex stainless steel, *Mater. Character.* **145**, 606–618 (2018)
2. Q. Li, Y. Kuang, W. Guo, et al., Experimental research on mechanical performance of SSRC columns under eccentric compression, *Appl. Sci.* **10**, 5629 (2020)
3. J. Magee, Development of Type 204 Cu stainless steel, a low-cost alternate to Type 304, *Wire J. Int.* **35**, 84–90 (2002).
4. C.S. Souza, R.B. Soares, R.A.D. de Faria et al., Effect of the prior cold work on the corrosion resistance of lean duplex stainless steel welded by GMAW process, *Mater. Corros.* **69**, 1548–1559 (2018)
5. G. Cai, Y. Huang, Effects of Ce addition on grain boundary character distribution, corrosion behavior and impact toughness of AISI 204Cu stainless steel, *J. Mater. Eng. Perform.* **28**, 3683–3694 (2019)
6. A. Kocijan, Corrosion behaviour of AISI 204Cu and AISI 304 stainless steels in simulated pore solution, *Int. J. Mater. Res.* **104**, 993–998 (2013)
7. F. Rosalbino, G. Scavino, G. Ubertalli, Passivity and its breakdown on low temperature plasma carburized AISI 204Cu stainless steel in chloride-containing solution, *Mater. Corros.* **69**, 563–571 (2018)
8. S. Raj, P. Biswas, Mechanical and microstructural characterizations of friction stir welded dissimilar butt joints of Inconel 718 and AISI 204Cu austenitic stainless steel, *Materials Characterization* **185**, 111763 (2022)
9. M.J. Joseph, M.A. Jabbar, Effect of aging process on the microstructure, corrosion resistance and mechanical properties of stainless steel AISI 204, *Case Stud. Construct. Mater.* **11**, e00253 (2019)
10. I. Shakhova, A. Belyakov, Z. Yanushkevich et al., On strengthening of austenitic stainless steel by large strain cold working, *ISIJ Int.* **56**, 1289–1296 (2016)
11. N. Tsuchida, Y. Morimoto, T. Tonan et al., Stress-induced martensitic transformation behaviors at various temperatures and their TRIP effects in SUS304 metastable austenitic stainless steel, *ISIJ International* **51**, 124–129 (2011)
12. N. Nakada, H. Ito, Y. Matsuoka et al., Deformation-induced martensitic transformation behavior in cold-rolled and cold-drawn type 316 stainless steels, *Acta Mater.*, **58**, 895–903 (2010)
13. L. Freire, X. R. Nóvoa, G. Pena et al., On the corrosion mechanism of AISI 204Cu stainless steel in chlorinated alkaline media, *Corros. Sci.* **50**, 3205–3212 (2008)
14. L.E. Company, *Stainless steels welding guide*, Books, 2003
15. M.F. McGuire, *Stainless steels for design engineers*, ASM International, 2008
16. M. Sowrirajan, S. Vijayan, M. Arulraj et al., Effect of austenitic stainless steel weld clad layers on conduction heat transfer across the walls of pressure vessels, *Proc. Inst. Mecha. Eng. C* **236**, 6667–6687 (2022)
17. L. Jeffus, *Welding principle and applications*, **58**, 629–644 (2012)
18. L.P. Karjalainen, T. Taulavuori, M. Sellman, et al., Some strengthening methods for austenitic stainless steels, *Steel Res. Int.* **79**, 404–412 (2008)
19. W. Karlsen, S. van Dyck, The effect of prior cold-work on the deformation behaviour of neutron irradiated AISI 304 austenitic stainless steel, *J. Nuclear Mater.* **406**, 127–137 (2010)
20. T. Shintani, Y. Murata, Evaluation of the dislocation density and dislocation character in cold rolled Type 304 steel determined by profile analysis of X-ray diffraction, *Acta Mater.* **59**, 4314–4322 (2011)
21. K. Kim, et al., Improvement of strength and impact toughness for cold-worked austenitic stainless steels using a surface-cracking technique, *Metals (Basel)* **8**, 932 (2018)
22. ASTM, ASTM E8/E8M standard test methods for tension testing of metallic materials, *Annual book of ASTM Standards*, no. C, 2021
23. ASTM, ASTM E384-2016: standard test method for Knoop and Vickers hardness of materials, *ASTM Standards*, 2016
24. F. Cardarelli, *Materials handbook — a concise desktop reference*, *Mater. Des.* **22**, 95–109 (2001),
25. ASTM G31 – 72, ASTM G31: standard practice for laboratory immersion corrosion testing of metals, *ASTM International*, 2004
26. N. Ghosh, P.K. Pal, G. Nandi, Parametric optimization of MIG welding on 316L austenitic stainless steel by grey-based Taguchi method, *Procedia Technol.* **25**, 1038–1048 (2016)
27. A. Asmare, R. Al-Sabur, E. Messele, Experimental investigation of friction stir welding on 6061-T6 aluminum alloy using Taguchi-based GRA, *Metals (Basel)* **10**, 1480 (2020)
28. R.J. Jassim, H.M. Lieth, R. Al-Sabur et al. Influence of welding parameters on optimization of the tensile strength and peak temperature in AISI 1020 alloy joints welded by SAW, *AIP Conf. Proc.* **2660**, 020042 (2022)
29. S.A.-R. Ahmed, H.F. Makki, Corrosion rate optimization of mild-steel under different cooling tower working parameters using Taguchi design, *J. Eng.* **26**, 174–185 (2019)
30. W. Chuaiphan, L. Srijaroenpramong, Evaluation of microstructure, mechanical properties and pitting corrosion in dissimilar of alternative low cost stainless steel grade 204Cu and 304 by GTA welding joint, *J. Mater. Res. Technol.* **9**, 5174–5183 (2020)

31. A.v. Bansod, A.P. Patil, A.P. Moon et al., Microstructural and electrochemical evaluation of fusion welded low-nickel and 304 SS at different heat input, *J. Mater. Eng. Perform.* **26**, 5847–5863 (2017)
32. H.M. Lieth, R. Al-Sabur, R.J. Jassim et al., Enhancement of corrosion resistance and mechanical properties of API 5L X60 steel by heat treatments in different environments, *J. Eng. Res.* **9**, 428–440 (2021)

Cite this article as: Haider Mahdi Lieth, Murtadha Abbas Jabbar, Raad Jamal Jassim, Raheem Al-Sabur, Optimize the corrosion behavior of AISI 204Cu stainless steel in different environments under previous cold working and welding, *Metall. Res. Technol.* **120**, 415 (2023)